Ferromagnetism of Single-Crystalline Cu$_2$O Induced through Poly(*N*-vinyl-2-pyrrolidone) Interaction Triggering d-Orbital Alteration

Do Yoon Kim,[†] Chang Woo Kim,[†] Jong Hwa Sohn,[†] Kyu Joon Lee,[‡] Myung Hwa Jung,[‡] Min Gyu Kim,[§] and Young Soo Kang*,[†]

[†]Korea Center for Artificial Photosynthesis and Department of Chemistry and [‡]National Creative Research Initiative Center for Superconductivity and Department of Physics, Sogang University, Seoul 121-742, Korea

[§]Beamline Research Division, Pohang Accelerator Laboratory, Pohang University of Science and Technology, Pohang 790-784, Korea

S *Supporting Information*

ABSTRACT: Ferromagnetic-like properties of cuprous oxide (Cu$_2$O) are induced through its interaction with chemisorbed surfactant poly(*N*-vinyl-2-pyrrolidone) (PVP), which alters the intrinsic d^{10} configuration of Cu ions. Structural and magnetism-related properties of intact Cu$_2$O crystals (i-Cu$_2$O) and those capped with PVP (c-Cu$_2$O) were examined using various analytical instruments. SEM, TEM (corresponding selected area electron diffraction (SAED)), and XRD of i-Cu$_2$O and c-Cu$_2$O showed cubic and hexagonal shapes of single crystallinity with facets of {200} and {111}, respectively, resulting from the differential growth rates of the original identical crystals along the facets over time. Bulk magnetic susceptibility (χ) of i-Cu$_2$O and c-Cu$_2$O at room temperature in field-dependent magnetization and the difference in their magnetic moment in temperature-dependent magnetization showed diamagnetic and ferromagnetic properties, respectively. The difference in the fluorescence mode of X-ray absorption near edge structure (XANES) spectra between i-Cu$_2$O and c-Cu$_2$O, showing no quadruple pre-edge peak for the transition 1s → 3d in Cu(II) ions with d^9 electronic configuration, indicates an orbital alteration on the surface of c-Cu$_2$O caused by an interaction with PVP. Two peaks for c-Cu$_2$O at higher binding energies in O 1s X-ray photoelectron spectroscopy may be indicative of the ligand-to-metal charge transfer (LMCT) from O atoms of PVP to Cu ions of Cu$_2$O, generating a chemical interaction through coordination bonding. Large hyperfine splitting constants in electron paramagnetic resonance (EPR) spectra of c-Cu$_2$O support this interpretation, with septet hyperfine splitting suggestive of Cu−Cu interactions on the surface of c-Cu$_2$O via the interaction with O atoms of PVP. These results demonstrate that PVP capping of Cu$_2$O crystal (c-Cu$_2$O) induces ferromagnetism of Cu(I) ions through coordination with O atoms of chemically adsorbed PVP. This may induce LMCT and Cu−Cu interactions that lead to changes in electronic configurations, deriving the ferromagnetic moments of c-Cu$_2$O.

N O (PVP) Cu
C O (Cu$_2$O)
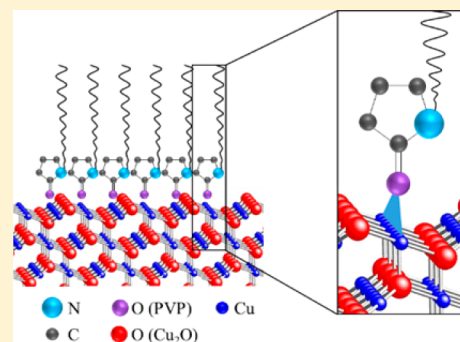
INTRODUCTION

Cuprous oxide, Cu$_2$O, is one of the most intensively studied semiconductors. It has recently been highlighted because of its large exciton binding energy of 140 meV and charge (minority) carrier properties with a mobility of ∼100 cm^2 V^{-1} s^{-1}.[1,2] These intrinsic properties make Cu$_2$O a promising material in the field of spintronics and optoelectronics.[3] However, it is a diamagnetic material with no intrinsic electron magnetic moments, restricting its usability in fabricating spintronic devices that rely on magnetic force rather than electrical currents.

Magnetism can be induced in diamagnetic materials by doping transition metal ions, resulting in a diluted magnetic semiconductor (DMS).[4−6] Cu$_2$O powders and films doped with Mn, Ni, or Co ions show ferromagnetism at room temperature (RT).[7−9] In addition, Cu$_2$O films co-doped with Al or Co ions show ferromagnetism at RT.[10] The Ruderman−

Kittel−Kasuya−Yosida (RKKY) interaction[11−13] in the DMS system is believed to explain the coupling exchange with the doped magnetic ions, and this interaction induces ferromagnetism.[14−16] However, undoped Cu$_2$O crystals exhibit a wide range of magnetism, from diamagnetism through paramagnetism to even ferromagnetism, which is generally derived from the existence of cationic vacancies in the lattice resulting from excess oxygen atoms generated during synthesis and manipulation of the Cu$_2$O samples.[17] An ab initio density functional theory (DFT) calculation suggests that the ferromagnetism can be observed with an increasing density of cationic vacancies in the intrinsic lattice of Cu$_2$O.[17] The experimental results also indicate that ferromagnetic properties of Cu$_2$O arise from the

existence of defects identical to cationic vacancies in the materials,[18−20] but the crystal structure of the semiconductor is distorted by the vacancies or implanted particles because of doping with other elements, possibly altering the semiconductive properties, although it is possible that the subsequent thermal annealing process eliminates such distortions produced in the crystal structure. However, this attempt to fabricate magnetic semiconductors by distorting its intrinsic network structure results in poor optoelectronics and spintronic devices that account for the decrease in long-range ordering, which decreases its own electron conductivity.[21]

Recently, it was found that the ferromagnetic behavior can be induced without doping of magnetic ions or native lattice defects (cationic vacancies) in single-crystalline semiconductors. Garcia et al. reported that nanoparticles of ZnO capped with organic molecules exhibit ferromagnetic behavior at RT despite the diamagnetic characteristic of the bulk metal. It was suggested that the surface defect induced by capping with organic materials strongly contributes to the alteration of intrinsic electronic configuration of d orbitals in ZnO nanoparticles.[22] Similar results on the ferromagnetic behavior were already reported with CdSe nanoparticles capped with thiols.[23]

Magnetism induced in semiconductors by capping with organic materials has great potential for spintronic and optoelectronic devices. However, there are few reports on the fabrication of ferromagnetic Cu_2O particles, the magnetic properties of which are induced by capping with organic material. Therefore, the purpose of this study was to induce ferromagnetic properties of Cu_2O single-crystalline particles capped with organic material, PVP, which functions as a ligand to bind through coordination bonding.

■ EXPERIMENTAL METHODS

Synthesis of Cu_2O Nanocrystals with and without PVP Capping. Cu_2O nanocrystals were synthesized following the modified precipitation method reported by Zhang et al.[24] For the synthesis of uncapped crystals, 50 mL of 0.01 M cupric chloride ($CuCl_2$, 97%, Aldrich) was supplemented with 5 mL of 2.0 M sodium hydroxide (NaOH, 97%, Daejung) with vigorous agitation at 900 rpm. When blackish-brown precipitation was produced within 30 min after incubation, 5 mL of 0.60 M ascorbic acid ($C_6H_8O_6$, 99.5%, Kanto Chemical, aqueous solution) was injected dropwise into the cupric chloride solution for the formation of i-Cu_2O nanocrystals with cubic shapes for less than 10 s. The color of the solution changed from blackish-brown to brick red in 3 h. Throughout the preparation process, the thermal condition was maintained at 55 °C. For the synthesis of c-Cu_2O, 2.7 g of poly(N-vinyl-2-pyrrolidone) (PVP, M_w = ∼29,000, Aldrich) was dissolved in 50 mL of 0.01 M $CuCl_2$ solution at 55 °C. The solution was stirred for 1 h to ensure that it was homogeneous. Then, 5 mL of 2.0 M NaOH was added to the $CuCl_2$ solution with vigorous stirring. The color of the solution changed from blue to dark brown. After stirring for another 30 min, 5 mL of 0.6 M ascorbic acid aqueous solution was added to the solution, and the color turned from dark-brown to brick red within 3 h, forming c-Cu_2O with a octahedral shape. All products with and without PVP capping were centrifuged at 5000 rpm for 5 min and washed several times with deionized water and ethanol, then dried at room temperature for 24 h in a vacuum oven.

Characterization. SEM with a cold field-emission scanning electron microscope (Hitachi S-4300, Tokyo, Japan) and X-ray

diffractometer (XRD) with Cu Kα radiation (λ = 1.54056 Å) of a Rigaku X-ray diffractometer operating at 40 kV and 150 mA at a scanning rate of 0.02° per step in the 2θ range of 20° ≤ 2θ ≤ 70° were used to characterize the size and morphology of as-prepared Cu_2O nanocrystals. TEM, with a JEM-2010 transmission electron microscope (JEOL, Japan) operated at 200 kV, was used to determine the crystallinity and morphology of the prepared nanocrystals. A superconducting quantum-interference device with vibrating sample magnetometer (SQUID-VSM) was used to determine the magnetic susceptibilities of Cu_2O crystals. X-ray absorption near edge structure (XANES) spectra were collected on BL10C (multi-pole-wiggler source) beamline in the Pohang Light Source (PLS-II) with operation of top-up mode at 3.0 GeV under a ring current of 200 mA. The X-ray absorption spectroscopy data were registered for the powder samples with uniform and proper thickness on the polyimide film in fluorescence mode with N_2-gas-filled ionization chambers for photon detectors. Higher-order harmonic contaminations were removed by detuning of the incident X-ray to reduce its intensity by ∼40%. Energy calibration was performed for each measurement using reference materials placed in front of the third ion chamber. To normalize experimental XANES spectra, data reductions were performed through the standard XAFS procedure. X-ray photoelectron spectroscopy (XPS) measurements were performed with a Sigma Probe (VG Scientific) using monochromatic Al Kα radiation (1486.6 eV). The shifts in binding energy of the XPS spectrum were corrected using the C 1s peak at 284.6 eV as a reference peak. EPR spectra were registered at 4 K using X-band CW-EPR (Bruker), operating in the high-frequency 9.5 GHz modulation mode of the magnetic field. The parameters of registered EPR spectra were obtained using computer analysis of the obtained experimental spectra.

■ RESULTS AND DISCUSSION

Structural Properties. Figure 1 shows SEM images, TEM images (corresponding selected area electron diffraction (SAED) patterns), and XRD patterns of the i-Cu_2O and c-Cu_2O crystals with facets of {200} and {111}, which were synthesized with and without PVP, respectively. Initial formation of the copper products is identical between Cu_2O crystals with and without PVP capping, which is processed by
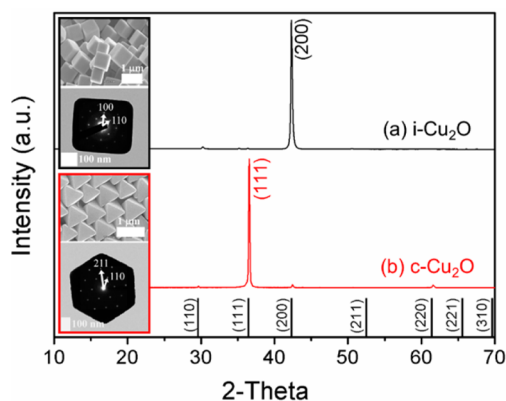

Figure 1. SEM, TEM images (with corresponding selected area electron diffraction (SAED) patterns), and XRD patterns of (a) cubic i-Cu_2O and (b) octahedral c-Cu_2O crystals. The black column indicates standard XRD patterns of Cu_2O (PDF 78-2076, ICDD, 1986).

the reduction of $Cu(OH)_2$ (product of $CuCl_2$ + NaOH) to Cu_2O in the presence of ascorbic acid. However, the different growth mechanisms of Cu_2O crystals with and without PVP capping were due to the different growth rates of various crystal facets caused by the selective suppression of PVP molecule adsorption of the crystal surface. Without PVP, the growth rate of the {111} facet was higher than that of the {100} facet because of the higher surface energy of the {111} facet relative to the {100} facet, resulting from exposure of the corresponding atoms on the surface (both O and Cu on {111} facet and only O on {100} facet).[24−26] As a result, crystal growth along the ⟨111⟩ direction occurs dominantly, leading to the final formation of the i-Cu_2O particles with the six surrounding {100} facets (Figure 1). With PVP, crystal growth along the ⟨111⟩ direction of the crystal surface was suppressed by the adsorbed polymer, PVP with −C=O residue in each monomer *N*-vinylpyrrolidone, which functions as a ligand to facilitate coordination bonding with Cu^{2+} ions. Thus, O atoms with lone pairs of electrons and negative dipoles could interact more favorably with an {111} facet because of Cu ions exposed on the surface. The {111} facet capped with PVP is stabilized and the surface reactivity of the {111} facet is also reduced. As a result of this stabilization, growth along the ⟨111⟩ direction is suppressed by adsorbed PVP, allowing dominant growth along the ⟨100⟩ direction.[24] As can be seen in the SEM images in Figure S1, the increasing concentration of PVP makes the Cu_2O crystal shape gradually undergo deformation from a cubic to octahedral shape. Cubes that are thermodynamically more stable form Cu_2O crystals more readily than octahedrons in the reaction solution in the absence of PVP. This was caused by the dominant growth of the {100} facet. When we used 1.68 g of PVP, truncated octahedral particles were produced. This may be derived from the partial adsorption of PVP on the {111} facet, resulting in the same growth ratio of the {111} and {100} facets. Finally, by increasing the amount of PVP to 2.7 g, c-Cu_2O crystals with six {111} facets were produced because of the predominant growth along the ⟨100⟩ direction.

XRD and TEM were used to characterize the single crystallinity of i-Cu_2O and c-Cu_2O. As can be seen from the XRD patterns of Figure 1, all specimens were matched with their Cu_2O standard (Powder Diffraction File (PDF) 78-2076, International Centre for Diffraction Data (ICDD), 1986). XRD patterns also clearly indicated that each {100} and {111} facet of cubic shaped i-Cu_2O and octahedral shaped c-Cu_2O, respectively, appeared on the surface of each particle.

TEM and corresponding SAED patterns (including FFT patterns and HRTEM of Figure S2) confirmed that both i-Cu_2O and c-Cu_2O crystals have single crystallinities. As shown in the XRD patterns of i-Cu_2O, the diffraction is indexed as [100] zone axis diffraction, which indicates that the surface of the top and bottom facets of single crystal are {100} facets; therefore the surrounding four vertical surfaces are also {100} facets. In contrast, the SAED pattern of single-standing c-Cu_2O is indexed as the [111] zone axis diffraction, which indicates that the both facets that are perpendicular to the zone axis are {111} facets.

Magnetic Properties. Field-dependent magnetic measurements were performed at T = 300 K with scanning fields from −70 to 70 kOe, and the data show the magnetization (M/H) curves corresponding to the diamagnetic properties of i-Cu_2O particles and ferromagnetic behavior of c-Cu_2O particles, respectively (Figure 2). In Figure 2a, the bulk magnetic susceptibility of i-Cu_2O (χ_I) was determined as χ_I = −0.858,
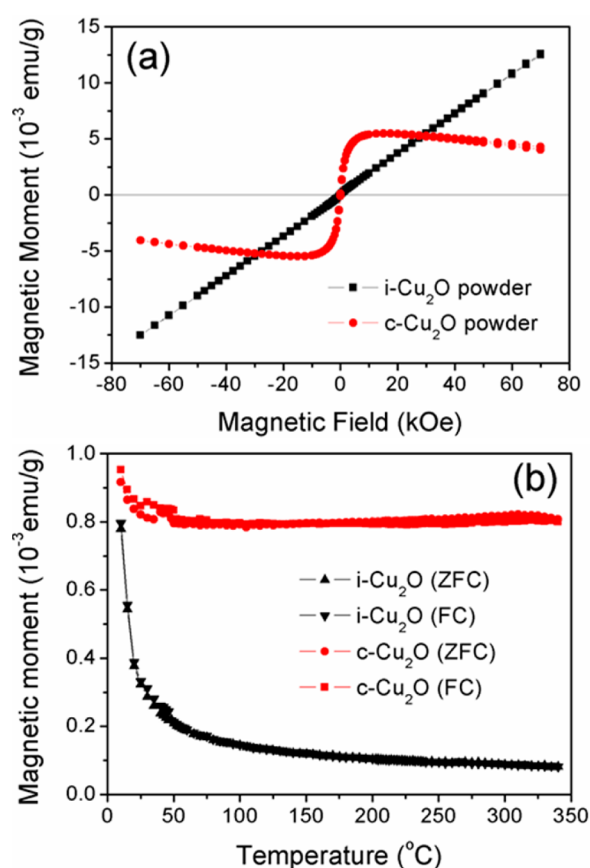
Figure 2. (a) Field-dependent magnetization curves of i-Cu_2O (black line with square dots) and c-Cu_2O (red line with round dots) at 300 K. (b) Temperature-dependent magnetization curves (340−10 K) under an applied field of 300 Oe in a zero-field-cooled (ZFC) and field-cooled (FC) i-Cu_2O (black line) and c-Cu_2O (red line).

indicating that the diamagnetic susceptibility of i-Cu_2O powder was similar to the intrinsic diamagnetic properties of pure Cu_2O. For the c-Cu_2O powder, the ferromagnetic susceptibility was determined to be χ_C = 1.053 and the diamagnetic background appeared with magnetic susceptibility of $\chi_{C,BKGD}$ = −1.002. In temperature-dependent magnetization (M/T) curves in Figure 2b, the increasing magnetization value of both particles at low temperature (∼50 K) represents the chance of having extrinsic impurities or cationic vacancies (intrinsic impurities) in the crystal lattice, resulting in the positive value of relative permeability (μ_I = 0.142) of the diamagnetic M/H curve of i-Cu_2O. In the present study, we used exactly the same precursors to prepare i-Cu_2O and c-Cu_2O particles in the absence and presence of PVP. The magnetic property of pure PVP results in diamagnetic properties in the electron paramagnetic resonance (EPR) spectra (Figure 5c, blue line). This indicates that both i-Cu_2O and c-Cu_2O particles should have ferromagnetic properties if the ferromagnetism originated from extrinsic impurities in Cu_2O precursors. In fact, there is no ferromagnetism in i-Cu_2O crystals; therefore, the ferromagnetism behavior of c-Cu_2O is not derived from extrinsic impurities, such as transition ions.

In addition, the thermal dependence of the magnetization suggests that intrinsic impurities are not the origin of the ferromagnetic properties of c-Cu_2O. It is known that the cationic vacancies (intrinsic impurities) in an inner lattice behave as paramagnetic, showing a gradual increase in

magnetization with decreasing temperature.[18] The degree of magnetization increases with the concentration of cationic vacancies with an increasing number of magnetic exchange interactions. For an increased magnetization value, from 50 to 10 K, the magnetic moment per gram resulted in 5.840×10^{-4} and 1.208×10^{-4} μ_B for i-Cu$_2$O and c-Cu$_2$O, respectively. Because the kinetics of crystal growth for two particles are different, the concentration of cationic vacancies (intrinsic impurities) in the two systems differed significantly. As a result of the lower increase in c-Cu$_2$O, cationic vacancies do not contribute to the ferromagnetism of c-Cu$_2$O compared with the diamagnetic properties of i-Cu$_2$O, which may have a higher concentration of cationic vacancies in its matrix. In addition, the diamagnetic background of c-Cu$_2$O supports this hypothesis. Moreover, structural analyses with TEM and XRD showed both i-Cu$_2$O and c-Cu$_2$O have single crystallinities, suggesting that the ferromagnetic behavior of the c-Cu$_2$O particles does not originate from the inner lattice defect. On the basis of these results, we conclude the magnetism is not due to magnetic or extrinsic impurities as well as intrinsic impurities.

Surface Interaction. Various analytical methods, such as XANES, XPS, IR spectroscopy, thermogravimetric analysis (TGA), and differential scanning calorimetry (DSC), have been used to investigate chemical functions of PVP capping in the alteration of electronic configurations.

X-ray absorption fine-structure measurement is a simple tool for obtaining electronic configuration information as well as direct evidence for lattice structure. No difference is observed in the transmittance mode of XANES spectra (not shown) for both i-Cu$_2$O and c-Cu$_2$O particles. This indicates that the lattice structure in the core component of both Cu$_2$O particles is close to the intrinsic lattice structure of Cu$_2$O. Figure 3 shows
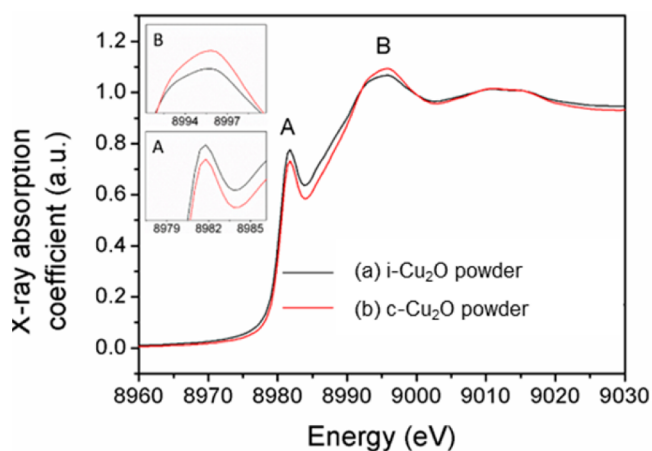
Figure 3. Cu K-edge XANES spectra of (a) i-Cu$_2$O and (b) c-Cu$_2$O powder. Peaks A and B of the spectrum indicate the 1s → 4p$_{x,y}$ and 1s → 4p$_z$ transitions, respectively.

the normalized Cu K-edge XANES spectra performed in fluorescence mode. Edge energy (E_0) can be determined from the maximum point of the first derivative function of each XANES spectra (Figure S3). Consequent results appear at the same edge energy E_0, 8980 eV. With the first and second derivatives of each signal considered, no pre-edge peak of quadruple transition 1s → 3d appears, which is usually shown in Cu(II) ions with d^9 electronic configuration. The absence of the pre-edge peak indicates that the electronic configuration of

both Cu ions in i-Cu$_2$O and c-Cu$_2$O are close to the d^{10} configuration.

Peaks A and B of the spectrum are assigned to the 1s → 4p$_{x,y}$ and 1s → 4p$_z$ transitions, respectively.[27−30] The linear coordination of Cu(I) ion with two O atoms along the z axis leads to ligand field-splitting of degenerated Cu 4p antiorbitals to 4p$_z$ and 4p$_{x,y}$. This coordination along the z axis increases the energy level of antibonding 4p$_z$ orbital to higher than 4p$_{x,y}$ orbitals. The intensity of the 1s → 4p$_z$ transition decreases because of covalent overlap with ligands along the z axis. For this reason, the peak for the 1s → 4p$_{x,y}$ transition would appear at a lower energy with higher intensity than the 1s → 4p$_z$ transition.[29,30] The spectra of i-Cu$_2$O particles show a higher intensity for peak A and lower intensity for peak B, indicating that i-Cu$_2$O particles have an ideal Cu$_2$O crystal and linear coordination of Cu ions compared with c-Cu$_2$O particles. In addition, we used fluorescence mode surface-dependent analysis, suggestive of a surface interaction between Cu ions and O atoms of PVP ligand on c-Cu$_2$O particles, which could induce alterations in the electronic configuration of Cu ions exposed on the surface.

Elemental composition of the Cu$_2$O crystal surface was analyzed using XPS (Figure 4). In Cu 2p XPS spectra, i-Cu$_2$O and c-Cu$_2$O particles showed a set of identical double peaks at higher (∼950 eV) and lower (∼930 eV) binding energies, indicative of minor changes in the elemental composition of Cu$_2$O on the crystal surface (Figure 4a). However, in O 1s XPS of i-Cu$_2$O and c-Cu$_2$O crystals and pure PVP, absorption peaks appeared at lower binding energies in a more or less broad feature centered at several binding energies (Figure 4b). In the O 1s XPS spectrum of c-Cu$_2$O particles (Figure 4b, red line), the two peaks at lower binding energies (528.11 and 529.54 eV) may coincide with two peaks of i-Cu$_2$O particles (Figure 4b, black line). However, two peaks for c-Cu$_2$O particles at higher binding energies of 532.08 and 533.56 eV may be related to O atoms of adsorbed PVP on the Cu$_2$O surface, which reveals that the O 1s binding energy of pure PVP (Figure 4b; blue line, 531.18 eV) shifted to a higher binding energy, indicating that ligand-to-metal charge transfer (LMCT) from the O atom of PVP to the Cu^{2+} ion of c-Cu$_2$O occurs through the coordination bonding between O atoms of the capping PVP molecule and Cu$_2$O surface through chemisorption.[31−34]

This suggestion can be supported on the basis of IR spectroscopy data. In our previous study on IR spectroscopy,[35] the IR spectrum of c-Cu$_2$O differentiated from that of pure PVP, indicating that the C=O stretch at 1647 cm^{-1} in the spectra of the crystal is red-shifted compared with that of pure PVP (1655 cm^{-1}) because of the weakening of the C=O bond in the carbonyl group of PVP. This indicates that the O atoms of capped PVP molecules are chemically coordinated with Cu ions on the surface of c-Cu$_2$O crystals.[31]

TGA and DSC provide supporting evidence for the chemisorption of PVP to Cu$_2$O crystal surface. As shown in Figure S4, the c-Cu$_2$O sample shows a wide range of temperature curves during the oxidation process (Cu$_2$O → CuO) at higher temperature ranges of 447−561 °C than those of the i-Cu$_2$O sample (321−448 °C), indicative of the chance for a chemical interaction via coordination bonding of PVP with the surface of c-Cu$_2$O crystals. Moreover, the weight ratios of the final CuO product oxidized from c-Cu$_2$O particles are lower than those from i-Cu$_2$O particles. This may be derived from the blocking or suppression effect of PVP adsorbed on c-Cu$_2$O particles on the external oxygen diffusion into the core
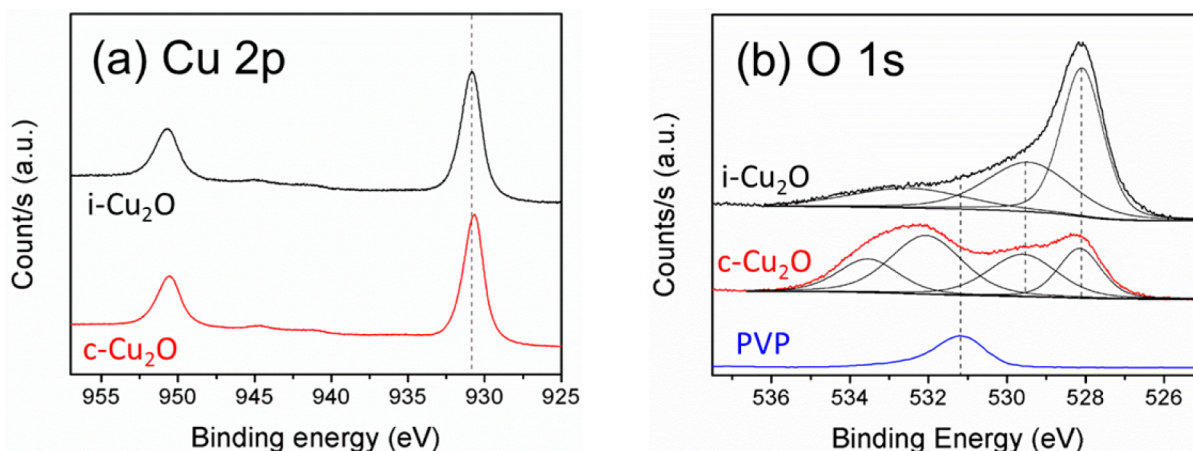
Figure 4. (a) Cu 2p XPS spectra of i-Cu_2O (black line) and c-Cu_2O (red line) particles. (b) O 1s XPS spectra of i-Cu_2O (black line) and c-Cu_2O (red line) particles and pure PVP (blue line).

area of Cu_2O particles accompanied by PVP decomposition. These results suggest that adsorption of PVP on the c-Cu_2O crystal surface leads to chemical coordination between the exposed Cu ions toward the surface of Cu_2O crystals and O atoms of PVP capping agent. This type of chemical coordination alters 3d orbital electronic configurations of Cu ions, thus resulting in its ferromagnetic properties.[22,31]

Electronic Configuration. EPR is powerful tool for investigating electronic configurations at low temperatures (4 K). As can be seen on the signal of i-Cu_2O particles in Figure 5a, there is no signal of unpaired electrons (electrons with unpaired magnetic moments), indicative of the diamagnetic properties of Cu(I) ions. For c-Cu_2O particles (Figure 5b),
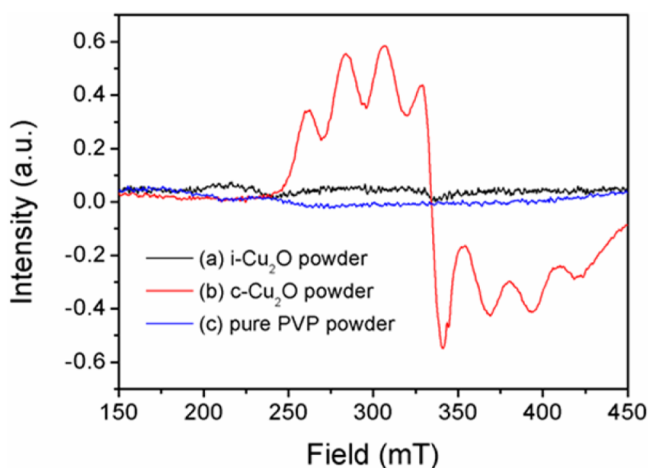
Figure 5. X-band electron paramagnetic resonance spectra of (a) i-Cu_2O, (b) c-Cu_2O, and (c) pure PVP powder at 4 K.

septet hyperfine splitting appeared with a g-value of 2.063 (Figure S6), which has little deviation in the range of g-value of conventional isotropic Cu^{2+} ($^2D_{5/2}$, $3d^9$) ion signal and hyperfine coupling constant of $A = 24.051$ mT, which appears at a larger value than in previous reports.[36−39] Cu has two isotopes, ^{63}Cu and ^{65}Cu, that exist naturally at an abundance of 69.1 and 30.9%, respectively. Signals from these two isotopes are not resolved because both have the same nuclear spin momentum. The septet hyperfine structure in the EPR signal readily indicates the presence of a nucleus with spin $I = 3$,

which would result from the Cu−Cu interaction (number of hyperfine structure = $2NI + 1$). In Cu^{2+} ionic compounds (for which $I = ^3/_2$) such as Cu_2O, septet hyperfine splitting can be obtained through the Cu−Cu interaction, as reported in previous studies.[36−39] With regard to single-crystalline properties of c-Cu_2O particles and chemical adsorption of PVP on their surface, the Cu−Cu interaction would be derived from the chemical coordination of O atoms of PVP on Cu ions of Cu_2O particles. In addition, single crystallinity of the particles supports discarding the Jahn−Teller distortion as a cause for the higher hyperfine coupling constant of Cu(I) ions, which would increase electron density at Cu(I) ions because of the decreased lattice spacing along the compressed axis. Meanwhile, it can be explained by LMCT from PVP to Cu(I) ions of Cu_2O surface, which is possible because of the electron-rich environment of PVP. The shift of O 1s XPS spectrum of PVP and corresponding IR spectroscopy data strongly support the LMCT from PVP to Cu_2O surface. Cu(I) ions would have higher electron density because of LMCT, additionally with an increased density of unpaired valence electrons of Cu(I) ions, causing the larger hyperfine-coupling constant.

■ CONCLUSIONS

Ferromagnetic behavior at RT in single-crystalline Cu_2O particles is induced by the d-orbital electronic configuration alteration of Cu(I) ions interacting with O atoms of PVP chemically coordinated with Cu ions on the crystal surface. As-synthesized i-Cu_2O particles have intrinsic properties of bulk Cu_2O. However, chemisorption of PVP on the c-Cu_2O surface could alter the electronic configuration of Cu(I) ions through charge transfer from O atoms of PVP to Cu(I) ions. Especially, orbital alteration would occur along the *xy*-orbital plane of Cu(I) ions and form the Cu−Cu interaction through O atoms of PVP, which appeared in the septet hyperfine splitting in the EPR spectrum of c-Cu_2O particles. As-prepared ferromagnetic Cu_2O was used for optoelectronic and spintronics devices with its outstanding electron conductivity accompanied by single crystallinity. In addition, the present study increases our understanding of the ferromagnetic behavior of Cu_2O particles induced by PVP capping.

■ ASSOCIATED CONTENT

Ⓢ Supporting Information

Further SEM, TEM, TGA/DSC, XRD, and EPR spectra as well as first and second derivatives of XANES spectra. The Supporting Information is available free of charge on the ACS Publications website at DOI: 10.1021/acs.jpcc.5b02762.

■ AUTHOR INFORMATION

Corresponding Author

*Tel.: +82-702-6379. E-mail: yskang@sogang.ac.kr.

Present Address

Y.S.K.: F 207, Sogang University, Seoul 121-742, Korea.

Notes

The authors declare no competing financial interest.

■ ACKNOWLEDGMENTS

■ ABBREVIATIONS

i-Cu_2O, Cu_2O crystal intact; c-Cu_2O, Cu_2O crystal capped with poly(*N*-vinyl-2-pyrrolidone); PVP, poly(*N*-vinyl-2-pyrrolidone)

■ REFERENCES

(1) Gou, L. F.; Murphy, C. J. Solution-phase synthesis of Cu_2O nanocubes. *Nano Lett.* **2003**, *3*, 231.

(2) Pearton, S. J.; Abernathy, C. R.; Overberg, M. E.; Thaler, G. T.; Norton, D. P.; Theodorpoulou, N.; Hebard, A. F.; Park, Y. D.; Kim, J.; Boatner, L. A. Wide band gap ferromagnetic semiconductors and oxides. *J. Appl. Phys.* **2003**, *93*, 1.

(3) Wolf, S. A.; Awschalom, D. D.; Buhrman, R. A.; Daughton, J. M.; von Molnar, S.; Roukes, M. L.; Chtchelkanova, A. Y.; Treger, D. M. Spintronics: a spin-based electronics vision for the future. *Science* **2001**, *294*, 1488.

(4) Schlafer, H. L.; Gliemann, G. *Basic principles of ligand field theory*; Wiley: New York, 1969; p 120.

(5) Erwin, S. C.; Zu, L.; Haftel, M. I.; Efros, A. L.; Kennedy, T. A.; Norris, D. J. Doping semiconductor nanocrystals. *Nature* **2005**, *436*, 91.

(6) Dietl, T.; Ohno, H. Engineering magnetism in semiconductors. *Mater. Today* **2006**, *9*, 18.

(7) Antony, J.; Qiang, Y.; Faheem, M.; Meyer, D.; McCready, D. E.; Engelhard, M. H. Ferromagnetic semiconductor nanoclusters: Co-doped Cu_2O. *Appl. Phys. Lett.* **2007**, *90*, 013106.

(8) Wei, M.; Braddon, N.; Zhi, D.; Midgley, P. A.; Chen, S. K.; Blamire, M. G.; MacManus-Driscoll, J. L. Room temperature ferromagnetism in bulk Mn-doped Cu_2O. *Appl. Phys. Lett.* **2005**, *86*, 072514.

(9) Ahmed, A.; Gajbhiye, N. S. Room temperature ferromagnetism in Mn, Ni and Co ions doped Cu_2O nanorods. *J. Solid State Chem.* **2010**, *183*, 3100.

(10) Kale, S. N.; Ogale, S. B.; Shinde, S. R.; Sahasrabuddhe, M.; Kulkarni, V. N.; Greene, R. L.; Venkatesan, T. Magnetism in cobalt-doped Cu_2O thin films without and with Al, V, or Zn codopants. *Appl. Phys. Lett.* **2003**, *82*, 2100.

(11) Ruderman, M. A.; Kittel, C. Indirect exchange coupling of nuclear moments by conduction electrons. *Phys. Rev.* **1954**, *96*, 99.

(12) Kasuya, T. Electrical resistance of ferromagnetic metals. *Prog. Theor. Phys.* **1956**, *16*, 58.

(13) Yoshida, K. Magnetic properties of Cu-Al alloys. *Phys. Rev.* **1957**, *106*, 893.

(14) Dietl, T.; Ohno, H.; Matsukura, F.; Cibert, J.; Ferrand, D. Zener model description of ferromagnetism in zinc-blende magnetic semiconductors. *Science* **2000**, *287*, 1019.

(15) Dietl, T.; Ohno, H.; Matsukura, F. Hole-mediated ferromagnetism in tetrahedrally coordinated semiconductors. *Phys. Rev. B* **2001**, *63*, 195205.

(16) Dietl, T. Origin of ferromagnetic response in diluted magnetic semiconductors and oxides. *J. Phys.: Condens. Mater.* **2007**, *19*, 165204.

(17) O'Keeffe, M.; Stone, F. S. The magnetochemistry and stoichiometry of the copper-oxygen system. *Proc. R. Soc. London, Ser. A* **1962**, *267*, 501.

(18) Chen, C. P.; He, L.; Lai, L.; Zhang, H.; Lu, J.; Guo, L.; Li, Y. D. Magnetic properties of undoped Cu_2O fine powders with magnetic impurities and/or cation vacancies. *J. Phys:. Condens. Mater.* **2009**, *21*, 145601.

(19) Liao, L.; Yan, B.; Hao, Y. F.; Xing, G. Z.; Liu, J. P.; Zhao, B. C.; Shen, Z. X.; Wu, T.; Wang, L.; Thong, J. T. L.; Li, C. M.; Huang, W.; Yu, T. P-type electrical, photoconductive, and anomalous ferromagnetic properties of Cu_2O nanowires. *Appl. Phys. Lett.* **2009**, *94*, 113106.

(20) Prabhakaran, G.; Murugan, R. Room temperature ferromagnetic properties of Cu_2O microcrystals. *J. Alloys Compd.* **2013**, *579*, 572.

(21) Fabian, J.; Matos-Abiague, A.; Ertler, C.; Stano, P.; Žutić, I. Semiconductor spintronics. *Acta Phys. Slovaca* **2007**, *57*, 565.

(22) Garcia, M. A.; Merino, J. M.; Fernández Pinel, E.; Quesada, A.; de la Venta, J.; Ruíz González, M. L.; Castro, G. R.; Crespo, P.; Llopis, J.; González-Calbet, J. M.; Hernando, A. Magnetic properties of ZnO nanoparticles. *Nano Lett.* **2007**, *7*, 1489.

(23) Lee, J. R. I.; Whitley, H. D.; Meulenberg, R. W.; Wolcott, A.; Zhang, J. Z.; Prendergast, D.; Lovingood, D. D.; Strouse, G. F.; Ogitsu, T.; Schwegler, E.; Terminello, L. J.; van Buuren, T. Ligand-mediated modification of the electronic structure of CdSe quantum dots. *Nano Lett.* **2012**, *12*, 2763.

(24) Zhang, D. F.; Zhang, H.; Guo, L.; Zheng, K.; Han, X. D.; Zhang, Z. Delicate control of crystallographic facet-oriented Cu_2O nanocrystals and the correlated adsorption ability. *J. Mater. Chem.* **2009**, *19*, 5220.

(25) Murphy, C. J. Materials science. Nanocubes and nanoboxes. *Science* **2002**, *298*, 2139.

(26) Wang, Z. L.; Feng, X. D. Polyhedral shapes of CeO_2 nanoparticles. *J. Phys. Chem. B* **2003**, *107*, 13563.

(27) Kau, L. S.; Spira-Solomon, D. J.; Penner-Hahn, J. E.; Hodgson, K. O.; Solomon, E. I. X-ray absorption edge determination of the oxidation state and coordination number of copper. Application to the type 3 site in *Rhus vernicifera* laccase and its reaction with oxygen. *J. Am. Chem. Soc.* **1987**, *109*, 6433.

(28) Kim, W. B.; Lee, J. S. Quantitative XANES analysis of cuprous dibromide complex formed in the oxidative carbonylation of phenols. *J. Phys. Chem. B* **2003**, *107*, 9195.

(29) Rothe, J.; Hormes, J.; Bonnemann, H.; Brijoux, W.; Siepen, K. In situ X-ray absorption spectroscopy investigation during the formation of colloidal copper. *J. Am. Chem. Soc.* **1998**, *120*, 6019.

(30) Moen, A.; Nicholson, D. G.; Ronning, M. Studies on the pre-edge region of the X-ray absorption spectra of copper (I) oxide and the diamminecopper(I) ion. *J. Chem. Soc., Faraday Trans.* **1995**, *91*, 3189.

(31) Xian, J.; Hua, Q.; Jiang, Z.; Ma, Y.; Huang, W. Size-dependent interaction of the poly(N-vinyl-2-pyrrolidone) capping ligand with Pd nanocrystals. *Langmuir* **2012**, *28*, 6736.

(32) Moulder, T. F.; Stickle, W. J.; Sobol, P. E.; Bomben, K. D. *Handbook of X-ray photoelectron spectroscopy*; PerkinElmer: Eden Prairie, MN, 1992.

(33) Elechiguerra, J. L.; Larios-Lopez, L.; Liu, C.; Garcia-Gutierrez, D.; Camacho-Bragado, A.; Yacaman, M. J. Corrosion at the nanoscale: The case of silver nanowires and nanoparticles. *Chem. Mater.* **2005**, *17*, 6042.

(34) Yao, K. X.; Zeng, H. C. ZnO/PVP nanocomposite spheres with two hemispheres. *J. Phys. Chem. C* **2007**, *111*, 13301.

(35) Sohn, J. H.; Cha, H. G.; Kim, C. W.; Kim, D. K.; Kang, Y. S. Fabrication of hollow metal oxide nanocrystals by etching cuprous oxide with metal(II) ions: approach to the essential driving force. *Nanoscale* **2013**, *5*, 11227.

(36) Ishikawa, Y.; Shigmatsu, K. Electron spin resonance in $Sr_{0.60}Ca_{0.40}CuO_2$. *J. Phys. Soc. Jpn.* **1992**, *61*, 3067.

(37) Bleaney, B.; Bowers, K. D. Anomalous paramagnetism of copper acetate. *Proc. R. Soc. London, Ser. A* **1952**, *214*, 431.

(38) Kokoszka, G. F.; Allen, H. C.; Gordon, G. Magnetic and optical spectra of copper monochloroacetate 2.4 hydrate. *J. Chem. Phys.* **1967**, *47*, 10.

(39) Punnoose, A.; Maurya, B. P.; Mathew, J.; Umar, M.; Haque, M. I.; Singh, R. J. EPR observation of Cu^{2+}-Cu^{2+} pairs in cupric oxide powders. *Solid State Commun.* **1993**, *88*, 195.